SPATIAL & TEMPORAL CHARACTERISTICS OF SOLAR RADIATION VARIABILITY

Richard Perez[1], Sergey Kivalov[1] and Thomas E. Hoff[2]

[1] ASRC, The University at Albany, Albany, NY, USA

[2] Clean Power Research, Napa, CA, USA

1. Introduction

Solar resource variability is a broad terminology that may be used to describe different aspects of the solar resource. For instance, some people may be referring to the variability of the resource from one year to the next in a given month or season (e.g., Gueymard & Wilcox, 2011). Others may be referring to the microclimatic variability of the solar resource from one location to another.

This article addresses the specific issue of ***the short-term variability*** – i.e., the "noise" caused by passing clouds. This aspect of variability is illustrated in figure 1 for a highly variable day in Napa, CA.

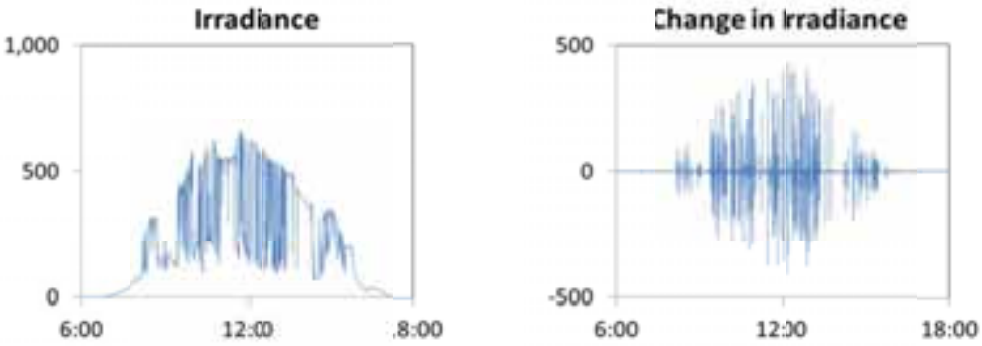

Fig. 1: Ten second irradiance at one location in Napa, CA on November 21, 2010

Following earlier work to model high frequency irradiances (e.g., see Skartveit & Olseth, 1992) to characterize the impact of variable conditions on the performance of transposition models (e.g., Vignola, 2001), the issue of short-term variability has recently emerged as a top concern for utility grid operators faced with prospects of large solar penetration. This concern has prompted a wealth of new research to better understand, parameterize and model its effects (e.g., see Sengupta et al., 2011, Lave et al., 2011, Frank et al., 2011, Kankiewicz et al., 2011, Hinkelman et al., 2011, Stein et al., 2011).

Key results relevant to the present investigation reported to this date by the authors and others include:

- Short-term variability includes two components: a predictable component caused by solar geometry (time of day / time of year) and a stochastic components caused by clouds and weather. The latter can be satisfactorily quantified by the time series of changes in clear sky indices (ratio between irradiance and clear sky irradiance). Most investigations have focused on the GHI clear sky index, Kt*, of relevance to flat plate solar technologies.
- Non-predictable short-term variability is mitigated when considering the combined output of distributed solar generators relative to a single one -- e.g., see empirical observations by Wiemken et al., 2001, Murata et al., 2009, Perez et al., 2009. This empirical evidence can be explained from probability theory's law of large numbers: the relative variability of a fleet of identical solar power plants decreases as the inverse of the square root of the number of plants when the individual plants' outputs are uncorrelated at the considered time scale (Hoff and Perez, 2010). The correlation that exists between individual plants is therefore a key parameter that determines the degree to which individual plants' fluctuations will add up or cancel out.
- The correlation between two individual locations depends upon the considered time scale and distance.

Mills & Wiser (2010) inferred such a trend by looking at one-minute measured data from the low density ARM network (Stokes & Schwartz, 1994). Perez et al. (2011) analyzed the same measured ARM network data but augmented the network's density by building one-dimensional high density virtual networks around each station. They derived a well-defined time-scale-distance relationships for 20 seconds to 15 minute fluctuations. Hoff & Perez (2011), looked at longer time scales (1-4 hours) for extended geographic areas using satellite derived data, confirming the solid trends but noting regional differences likely traceable to local cloud transit speed. They posited that a correlation function linking distance, time scale and cloud speed would likely be applicable down to scales of seconds.

In this paper, we take advantage of a new modeling technique capable of generating high resolution (1 km) high frequency (one-minute) irradiance data from geostationary satellites to complement and unify the above findings. The results show that a strong, predictable and site-independent site-pair correlation relationship exists between distance, considered fluctuation time scale, and local mean cloud transfer speed.

2. Variability Metrics

The non-deterministic component of solar resource variability is the results of short-term weather effects: passing and evolving cloud fields. The clear sky index Kt* defined as the ratio between global horizontal irradiance GHI and clear sky global irradiance GHI_{clear} is largely independent of solar geometry and is used to quantify this non-deterministic variability.

Hoff and Perez (2010) have previously quantified variability as the standard deviation of the time series of changes in Kt* from one time interval Δt to the next: $\sigma(\Delta kt^*_{\Delta t})$. This metric is retained for the present investigation.

3. Satellite-Derived One-Minute Irradiance Data

3.1. Methodology

The GOES geostationary satellites produce data on a half-hour basis with a ground resolution of 1 km at nadir for the visible channel. This channel is the main input to irradiance models such as the model of Perez et al. (2002) used in SolarAnywhere (2011).

The one-minute data are generated from the half-hour satellite-modeled irradiances by applying a methodology developed for cloud motion forecasts (Heinemann, et al., 2006, Perez et al., 2010) to points of time between satellite frames. Cloud motion is determined from two consecutive images; the motion assigned to each image pixel is the one that minimizes the local cloud pattern difference between the two images. Because they are initiated from known cloud field structures, cloud motion-based forecasts have been found to perform better than numerical weather prediction forecast models up to 4-5 hours ahead (Perez et al., 2010). Beyond this time horizon, performance degrades because cloud speeds evolve over time and space, and because the method does not account for cloud formation or cloud dissipation.

The cloud motion forecast methodology is applied here to simulate evolving cloud patterns at any time between two consecutive satellite images at time t_0 and t_1, respectively. Forward forecast is applied to the t_0 image, while backward forecast is applied to the t1 image by reversing motion vectors. The resulting cloud field at time t_i (with $t_0 < t_i < t_1$) is a weighted average between the forward and backward forecasts. The achievable time resolution Δt_{limit} is a function of the image's spatial resolution, Δx, which defines the size of the cloud structures that can be captured to determine variability at a given time scale, and of the cloud speed CS:

$$\Delta t_{limit} = \Delta x / CS \qquad \text{(eq. 1)}$$

For this study we use the native visible channel spatial resolution of ~ 1 km, allowing us to push the temporal resolution down to near one-minute for cloud speeds approaching 60 km/h. For lower speeds at that frequency, the one-minute generator should underestimate variability and overestimate site pair correlation -- however both variability and correlation observed at these low speeds can be corrected as discussed below.

Figure 2 illustrates 31 satellite-derived clear sky index frames over a ~ 200 km x 150 km region in northern California. The first and last frames are derived from actual satellite images while all the intermediate frames are produced using the methodology outlined above.

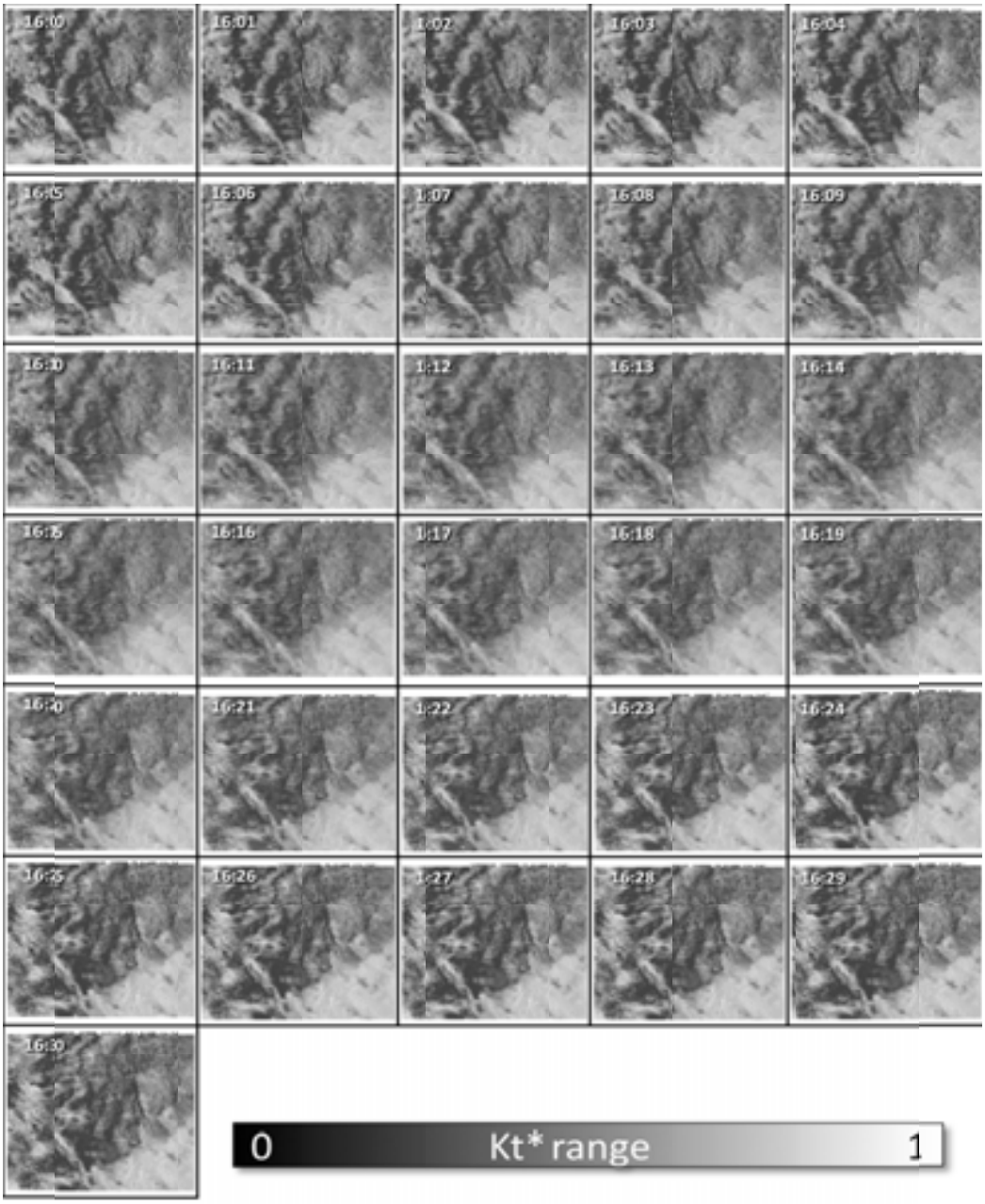

Fig. 2: One-minute satellite-derived Kt* in a 4x4 degree region in northern California. The first and last frames (16:00 and 16:30 GMT) are derived from actual satellite images. All the intermediate frames are derived from applying pixel-specific cloud motion vectors to the first and last frames3.2. Evaluation of the Methodology

The ability of the one-minute satellite derived irradiances to recreate variability conditions observed at the ground was gauged against one-minute measured GHI data from the ARM network's central facility in Oklahoma (Stokes & Schwartz, 1994) and against recent field measurements from a high density, high frequency mobile network that operated for a few days at Cordelia Junction near San Francisco, CA (Hoff and Norris, 2010). This network comprises 25 stations within a 400x400 meter footprint.

ARM Data: In Figure 3, we compare satellite derived one-minute Δkt* to measured Δkt* at the ARM central facility for the month of October, 2010. The top portion of the figure reports the ground and satellite Δkt* time series. The bottom part of figure 3 plots the sorted absolute values of ΔKt* for the 1,000 highest one-minute ramp rates observed during the 31 day period.

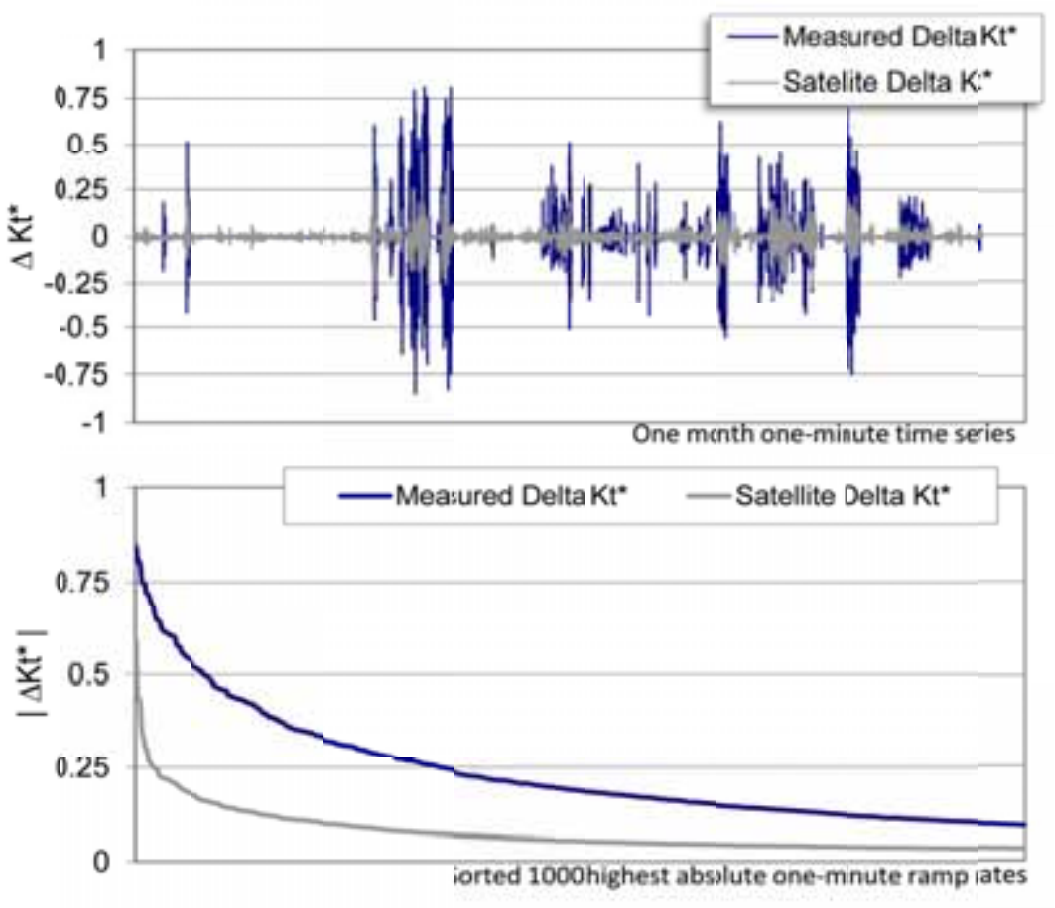

Fig. 3: comparing satellite derived and ground measured time series of Δkt* and sorted absolute ramp rates at the ARM Central facility

Satellite-derived one-minute variability is less than observed and appears to fall short of expectations. Indeed, the satellite derived variability quantified by Δkt*over that period is 40% of measured variability. There are two reasons for this lower satellite-derived variability: (1) the effective cloud speed for the month during the high variability days averaged 28 km/h, putting one-minute time step below the optimal Δt_{limit}, and (2) the satellite pixel does not represent one single station but an extended area. Per Hoff & Perez, 2010 such an extended area should exhibit less variability than a single location because its dispersion factor is larger than unity. Perez et al. (2011) derived an estimate of station pair variability correlation as a function of their distance for one minute data (see their fig. 4); applying this correlation function to a large number of single stations equally spaced over a 1x1 km foot print representing a satellite pixel and solving the correlation matrix (Hoff and Perez., 2011) indicates that the variability of the satellite extended pixel should be 60-70% of a single point's variability. The combined impact of both factors accounts for the scale of the difference shown in figure 3.

Cordelia Junction Data: This network operated for a few days in November 2010 in a 400x400m configuration. For this evaluation, we selected the highest variability day, November 10, and compared the satellite-derived variability to (1) the variability of one single station in and (2) the variability of the entire 25-station network -- the effective cloud speed for that day was ~ 35 km/h. In figure 4 we plotted the sorted 100 highest one-minute ramp rates' absolute values recorded for that day. The figure shows that the one-minute variability detected by the satellite is smaller than the variability of any single measuring station in the network, but also shows that it is nearly identical to the variability integrated over the network.

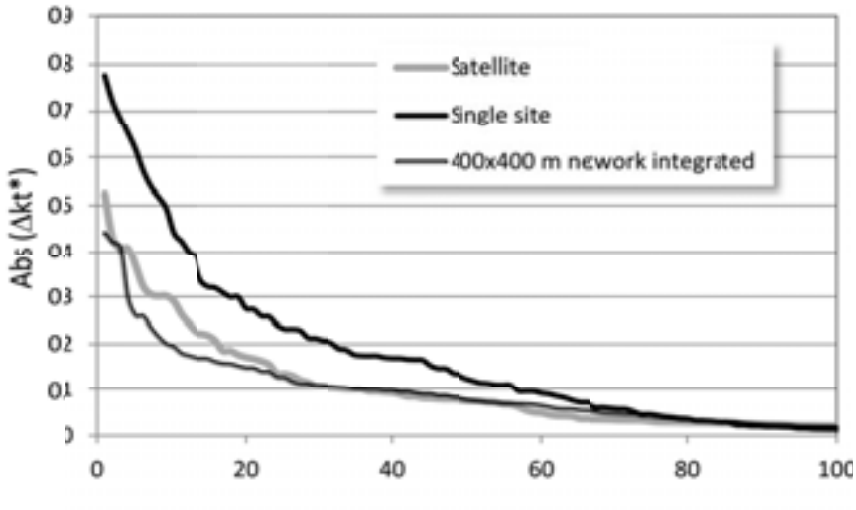

Fig. 4: Comparing satellite-derived and measured sorted absolute ramp rates at the Cordelia Junction network site

4. Results

All One-minute one-kilometer satellite-derived irradiances were produced for a four-month period in each of the five regions shown in figure 5. Four of the regions are 3 x 3 degrees in size – i.e., representing 90,000 high resolution satellites data points. They cover respectively central California, Nevada, the southern Great Plains and Hawaii. In addition, we also considered a 2 x 2 degrees subset of the Hawaii region focusing on the land area of the big island.

Fig. 5: Selected regions of satellite high-resolution one minute data production

4.1 Correlation of Δkt as a Function of Distance*

Thirty six uniformly distributed high resolution data points were selected within the central area of each region – each central area represents 2x2 degrees for the five large regions and 1x1 degrees for the small Hawaii region.

The correlation of the Δkt*time series between each of the 36 selected points and a random sample of all its possible neighbors within a 50 km radius was individually calculated for each month and each region -- the random sampling of neighbors reduced the number station pairs analyzed per region from 280,000 possible pairs down to a manageable 28,000. The random selection process was adjusted so as to keep the number of pairs analyzed within any particular distance range nearly constant.

Figure 6 illustrates observed site pair correlations as a function of distance and Δt for one sample month in each region analyzed. The considered Δt intervals range from one minute to one hour. The familiar trends previously noted by Hoff & Perez (2011), Perez et al. (2011), and Mills & Wiser (2010) based upon different empirical evidence (respectively hourly satellite data, virtual networks and low resolution networks) are qualitatively reproduced in the present analysis. In addition, it is clearly apparent that the rate of correlation decrease as a function of distance depends upon the prevailing regional cloud speed as had been inferred by Hoff and Perez's analysis of hourly satellite data (2011). The influence of cloud speed becomes more noticeable as Δt increases – which may explain why this effect was noted in Hoff & Perez analysis as they considered Δt's ranging from one hour to 4 hours and not in the virtual network analysis that considered Δt's ranging from 20 seconds to 15 minutes

The slight negative correlation noted by Perez et al. in the virtual network analysis (2011), and partially visible in high resolution network data (Hoff & Perez, 2011) is not reproduced through this analysis. The main causes of the observed negative correlation minimum were likely the one-dimensional nature of the virtual network and the assumed conservation of cloud structures.

We made no attempts at observing the influence of cloud speed direction vs. the considered distance on the observed correlation trends -- a slight, but noticeable variation to this effect has been noted by Hinkelman et al. (2011) which may be materialized here as the scatter around the observed trends in Fig. 6.

All the trends observed at all time scales and sites converge towards zero asymptotically with a convergence distance increasing with both Δt and cloud speed. Because the correlation zero cross-over noted in the virtual network analysis does not occur here, let's consider the 20% crossover threshold as an effective quantifier of the distance where the Δkt* time series at two locations are effectively uncorrelated. Figure 7 reports this effective decorrelation distance, x_{edd}, as a function of mean monthly cloud speed and Δt for each of the 20 site-months analyzed.

As conjectured above, the points reported in Figure 7 where Δt is below Δt_{limit} should overestimate the crossover distance. This effect is clearly apparent in Figure 8; according to Hoff and Perez's definition of the dispersion factor (2010), the station distance at any given correlation level divided by Δt and by the cloud speed should be a constant. The points where $\Delta t << \Delta t_{limit}$ are above the other data points, increasingly so as $\Delta t_{limit} / \Delta t$ increases. However, it is possible to use this observation and Hoff & Perez's dispersion factor definition to correct the concerned data points by bringing them to the level of the mean of all other points where $\Delta t > \Delta t_{limit}$. Doing so allows us to derive Figure9 identifying the effective 20% decorrelation distance as a function of prevailing cloud speed and Δt, and to propose the following equation for this effective distance:

$$x_{edd} = 1.5 \ \Delta t \ CS \qquad \text{(eq. 2)}$$

Figure 10 compares the application of equation (2) to the preliminary relationship identified in the virtual network analysis (Perez et al., 2011)

Further, recalling that x_{edd} correspond to 20% correlation threshold, and assuming, based on the present empirical evidence, that correlation decreases exponentially with distance, it is possible to use equation (2) to estimate any station pair correlations, C_{pair}, as a function of their distance, x, the fluctuation time scale Δt and the cloud speed CS per equation (3):

$$C_{pair} = \exp (x \ln 2 / 1.5 \ \Delta t \ CS) \qquad \text{(eq. 3)}$$

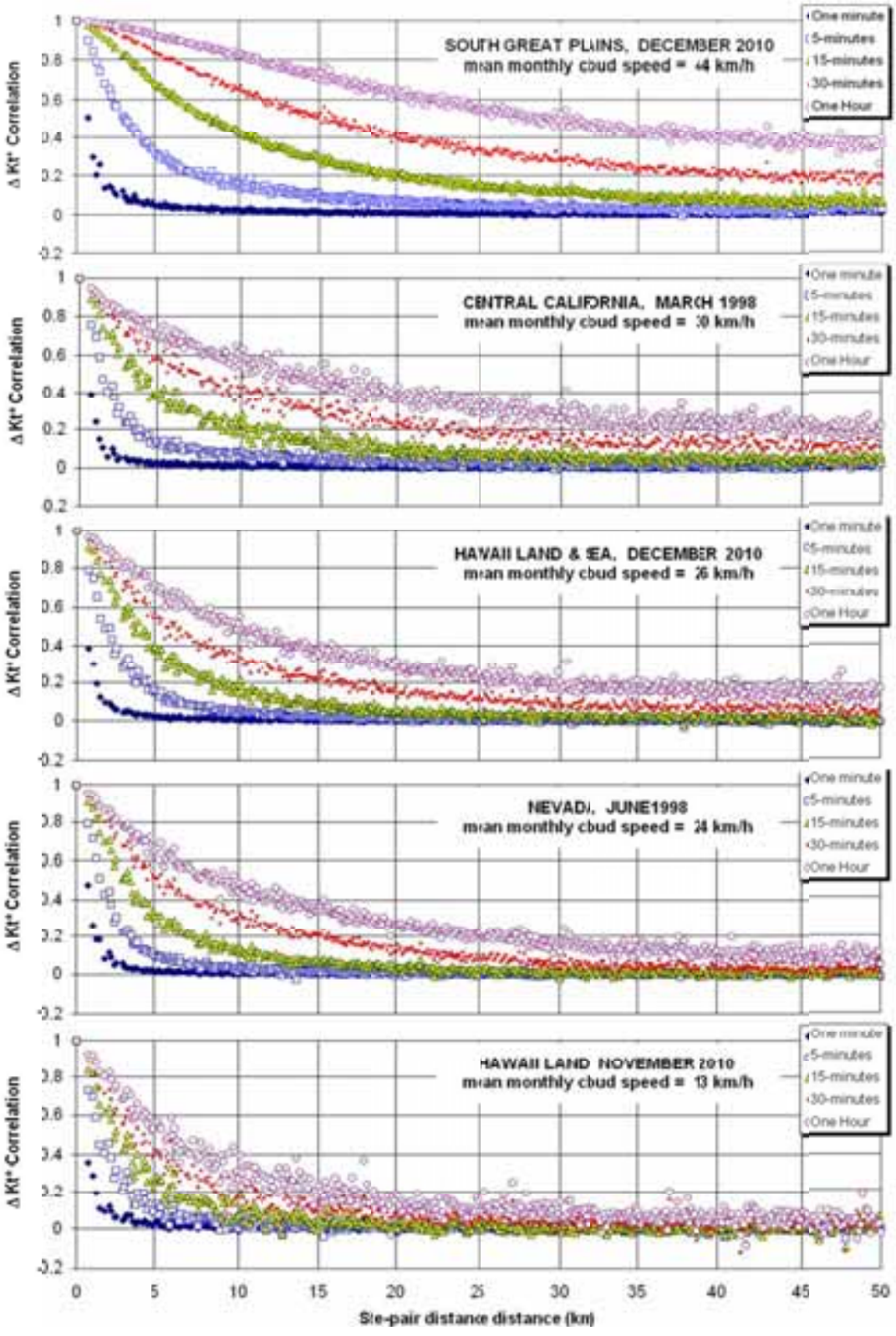

Fig. 6: Examples of site pair correlation as a function of distance for each region

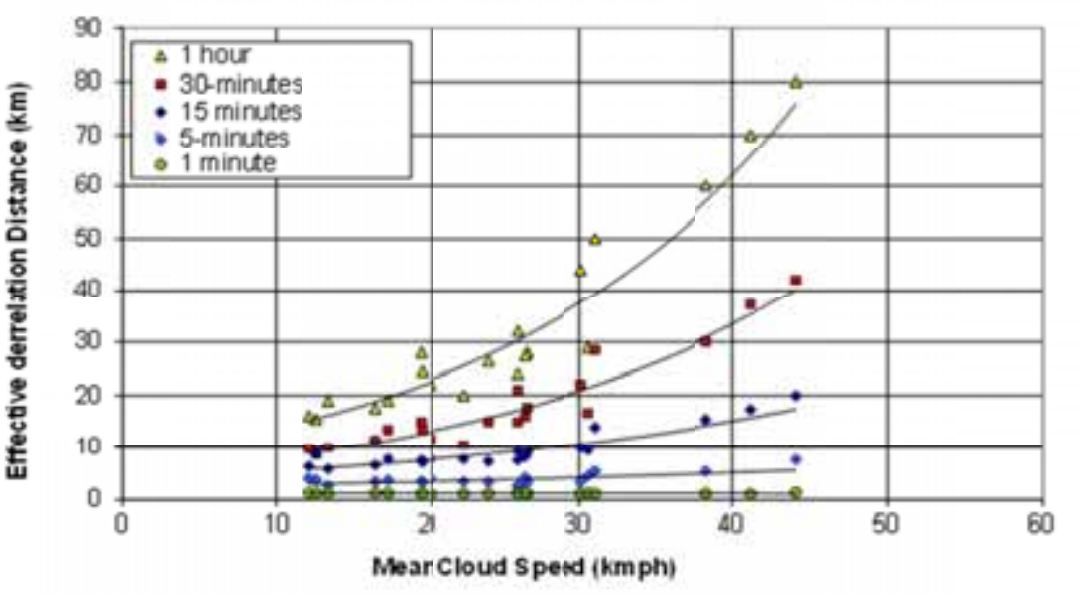

Fig. 7: Effective20%-threshold decorrelation distance as a function of mean monthly cloud transfer speed for each region/month analyzed

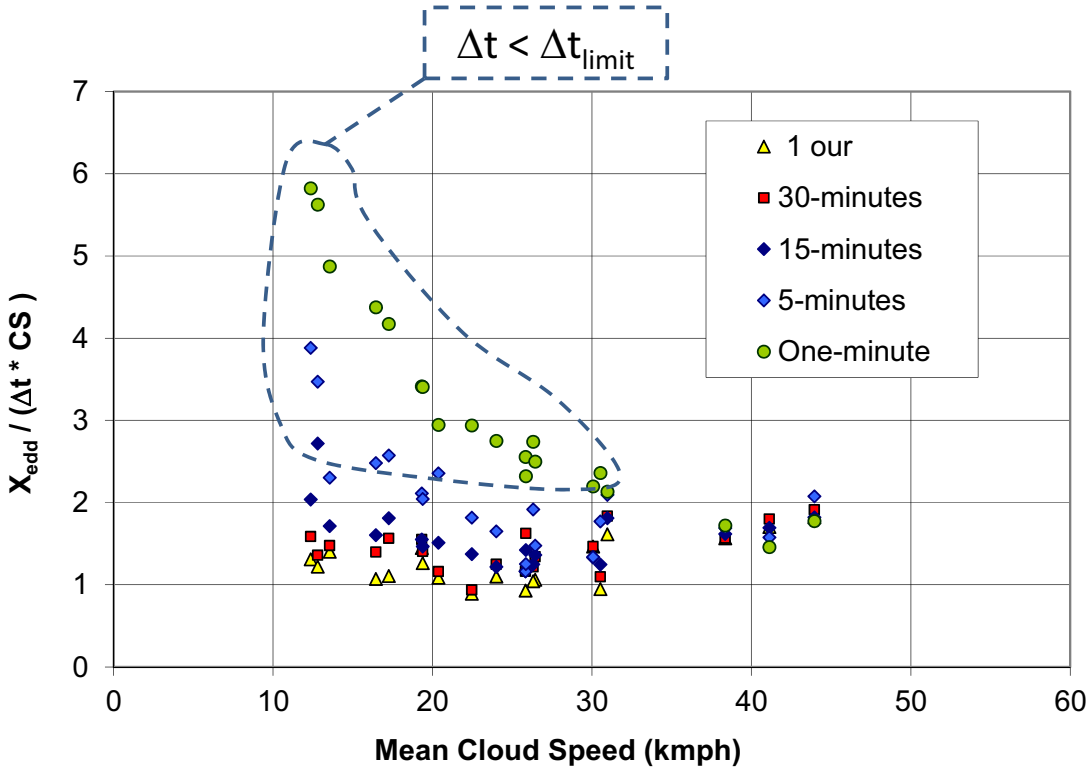

Fig. 8: Ratio between the observed effective decorrelation distance and the product of cloud speed and the considered fluctuation time scale as a function of cloud speed

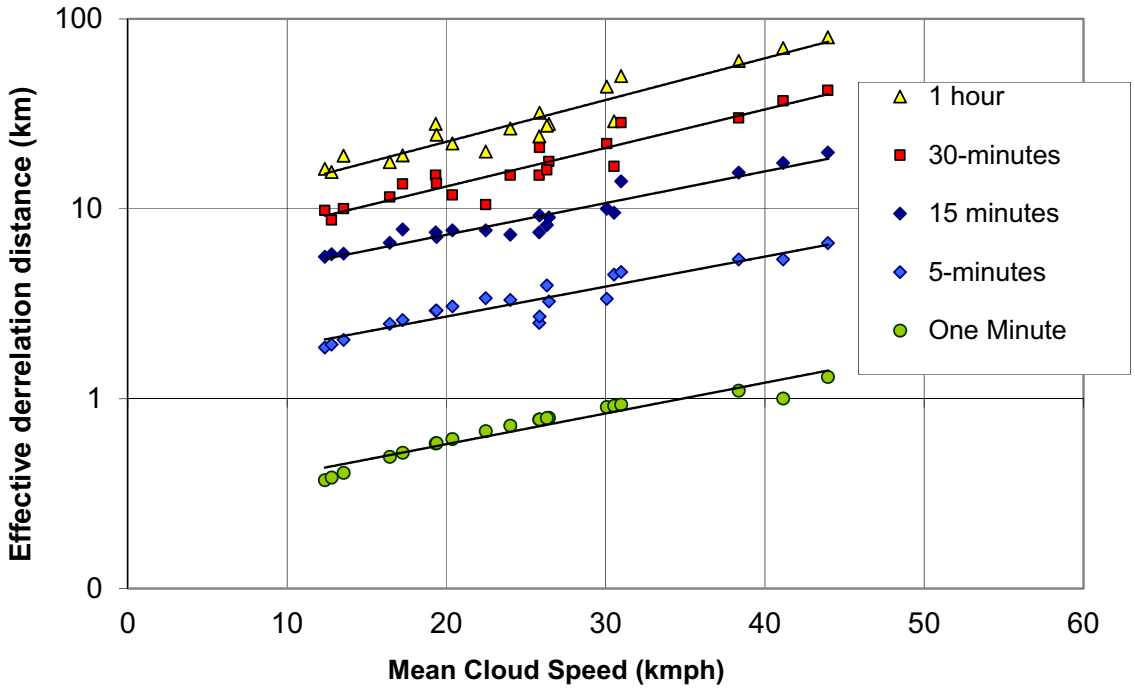

Fig. 9 : Corrected effective 20%-threshold decorrelation distance as a function of mean monthly cloud transfer speed for each region/month analyzed

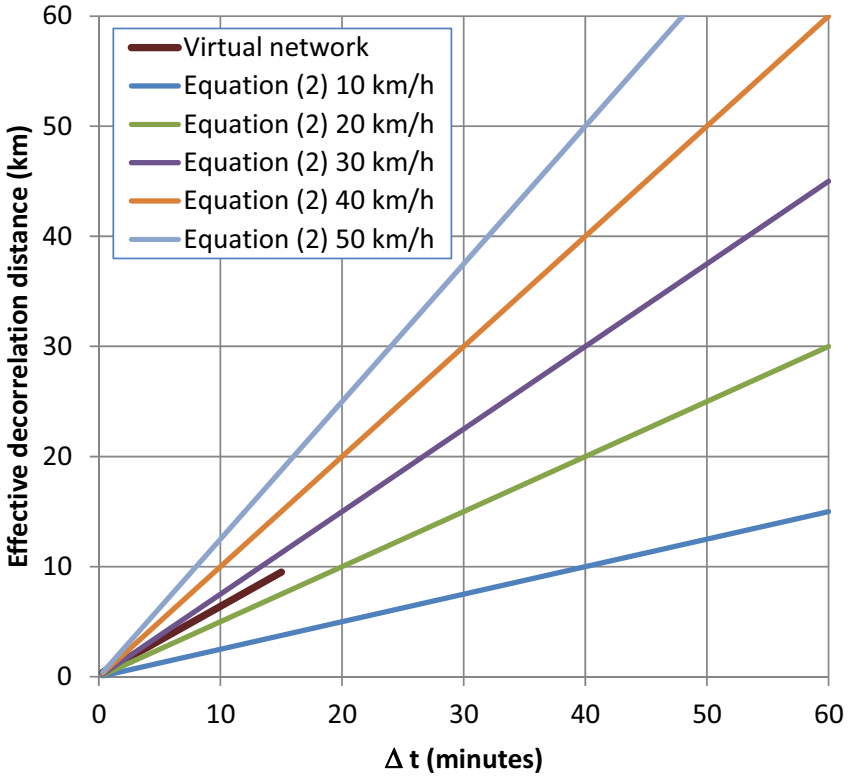

Figure 10: Comparing application of equation (2) for different cloud speeds against the virtual network derived trend from Perez et al., 2011

5. Conclusions

In this article we have presented experimental evidence showing that the short-term variability correlation observed between two locations is a predictable function of their distance, the considered fluctuation time scale and the local cloud speed. This experimental evidence was used to propose a simple model relating correlation to all three parameters.

As explained by Hoff and Perez, 2011, this relationship can be used, in conjunction with satellite-derived cloud motion vectors (see Perez et al., 2010) to build a correlation matrix for any arbitrarily deployed fleet of PV installations, and therefore to estimate their combined variability at any time scales.

6. Reference

Frank, J., J. Freedman, M. Brower and M. Schnitzer, 2011: Development of High Frequency Solar Data, Proc. Solar 2011, American Solar Energy Society Conf., Raleigh, NC

Gueymard C. and S. Wilcox, (2011): Assessment of spatial and temporal variability in the US solar resource from radiometric measurements and predictions from models using ground-based or satellite data. Solar Energy, 85, 5, 1068-1084

Heinemann, D., Lorenz, E., Girodo, M.: 2006, 'Solar irradiance forecasting for the management of solar energy systems', Solar 2006, Denver, CO (USA), 07.07.2006

Hinkelman L., R. George and M. Sengupta, 2011: Differences between Along-Wind and Cross-Wind Solar Variability. Proc. Solar 2011, American Solar Energy Society Conf., Raleigh, NC

Hoff, T. E., Perez, R. 2010. Quantifying PV power Output Variability. Solar Energy 84 (2010) 1782–1793

Hoff, T. E., Perez, R. 2011: Modeling PV Fleet Output Variability, Submitted to Solar Energy

Hoff, T.E., Norris, B. 2010. Mobile High-Density Irradiance Sensor Network: Cordelia Junction Results

Kankiewicz A., M. Sengupta and J. Li, 2011: Cloud Meteorology and Utility Scale variability. Proc. Solar 2011, American Solar Energy Society Conf., Raleigh, NC

Lave M. and J. Kleissl, 2011: Solar Variability over Various Timescales using the Top Hat Wavelet. Proc. Solar 2011, American Solar Energy Society Conf., Raleigh, NC

Mills, A., Wiser, R. 2010. Implications of Wide-Area Geographic Diversity for Short-Term Variability of Solar Power. Lawrence Berkeley National Laboratory Technical Report LBNL-3884E

Murata, A., H. Yamaguchi, and K. Otani (2009): A Method of Estimating the Output Fluctuation of Many Photovoltaic Power Generation Systems Dispersed in a Wide Area, Electrical Engineering in Japan, Volume 166, No. 4, pp. 9-19

Perez R., P. Ineichen, K. Moore, M. Kmiecik, C. Chain, R. George and F. Vignola, (2002): A New Operational Satellite-to-Irradiance Model. Solar Energy 73, 5, pp. 307-317

Perez, R., M. Taylor, and T. E. Hoff, J.P. Ross (2009): Redefining PV Capacity. Public Utilities Fortnightly, Volume 147, No. 2.

Perez R., S. Kivalov, J. Schlemmer, K. Hemker Jr., D. Renné and T. Hoff (2010) : Validation of Short and Medium Term Operational Solar Radiation Forecasts in the US. Solar Energy 84, 12, 2161-2172

Perez, R., Kivalov, S., Schlemmer, J., Hemker Jr., C. , Hoff, T. E. 2011. Short-term irradiance variability correlation as a function of distance. Proc. Solar 2011 American Solar Energy Society Conf. & Submitted to Solar Energy

Sengupta, 2011: Measurement and Modeling of Solar and PV Output Variability. Proc. Solar 2011, American Solar Energy Society Conf., Raleigh, NC

Skartveit A., and J. A. Olseth, (1992): The Probability Density of Autocorrelation of Short-term Global and beam irradiance. Solar Energy, Volume 46, No. 9, pp. 477-488.

Solar Anywhere, 2011, Web-Based Service that Provides Hourly, Satellite-Derived Solar Irradiance Data Forecasted 7 days Ahead and Archival Data back to January 1, 1998. www.SolarAnywhere.com

Stein, J., A. Ellis, C. Hansen, V. Chadliev, 2011: Simulation of 1-Minute Power Output from Utility-Scale Photovoltaic generation Systems. Proc. Solar 2011, American Solar Energy Society Conf., Raleigh, NC

Stokes, G.M., Schwartz, S.E., 1994. The atmospheric radiation measurement (ARM) program: programmatic background and design of the cloud and radiation test bed. Bulletin of American Meteorological Society 75, 1201–1221

Vignola, F., (2001): Variability of Solar Radiation over Short Time Intervals, Proc. Solar 2001, American Solar Energy Society Conf., Washington, D.C.

Wiemken E., H. G. Beyer, W. Heydenreich and K. Kiefer (2001): Power Characteristics of PV ensembles: Experience from the combined power productivity of 100 grid-connected systems distributed over Germany. Solar Energy 70, 513-519.